ARTICLE

https://doi.org/10.1038/s41586-019-0897-9

A dissipatively stabilized Mott insulator of photons

Ruichao Ma[1]*, Brendan Saxberg[1], Clai Owens[1], Nelson Leung[1], Yao Lu[1], Jonathan Simon[1] & David I. Schuster[1]

Superconducting circuits are a competitive platform for quantum computation because they offer controllability, long coherence times and strong interactions—properties that are essential for the study of quantum materials comprising microwave photons. However, intrinsic photon losses in these circuits hinder the realization of quantum many-body phases. Here we use superconducting circuits to explore strongly correlated quantum matter by building a Bose–Hubbard lattice for photons in the strongly interacting regime. We develop a versatile method for dissipative preparation of incompressible many-body phases through reservoir engineering and apply it to our system to stabilize a Mott insulator of photons against losses. Site- and time-resolved readout of the lattice allows us to investigate the microscopic details of the thermalization process through the dynamics of defect propagation and removal in the Mott phase. Our experiments demonstrate the power of superconducting circuits for studying strongly correlated matter in both coherent and engineered dissipative settings. In conjunction with recently demonstrated superconducting microwave Chern insulators, we expect that our approach will enable the exploration of topologically ordered phases of matter.

The richness of quantum materials originates from the competition between quantum fluctuations arising from strong interactions, motional dynamics and the topology of the system. The results of this competition manifest as strong correlations and entanglement, which are observed both in the equilibrium ground state and in non-equilibrium dynamical evolution. In most condensed matter systems, efficient thermalization to a cold reservoir that has a well-defined chemical potential leads naturally to the preparation of the system near its many-body ground state, so understanding of the path to strong correlations—how particles order themselves under the system Hamiltonian—is limited.

Synthetic quantum materials provide an opportunity to investigate this paradigm. Built from highly coherent constituents with precisely controlled and tunable interactions and dynamics, such materials have emerged as ideal platforms to explore quantum correlations, owing to their slowed dynamics and in high-resolution-imaging capabilities[1,2]. Low-entropy strongly correlated states are typically reached adiabatically in a many-body analogue of the Landau–Zener process by slowly tuning the system Hamiltonian through a quantum phase transition while the system is isolated from the environment, starting with a low-entropy state prepared in a weakly interacting or weakly correlated regime. As a prominent example from atomic physics, laser and evaporative cooling remove entropy from weakly interacting atomic gases to create Bose–Einstein condensates[3,4], which are then used to adiabatically reach phases such as Mott insulators[5], quantum magnets[6,7] and potentially even topologically ordered states[8]. These coherent isolated systems have prompted studies of relaxation in closed quantum systems, including observation of pre-thermalization[9], many-body localization[10] and quantum self-thermalization[11]. Nonetheless, the challenge in such a 'cool, then adiabatically evolve' approach is the competition between the limited coherence time and the adiabatic criterion at the smallest many-body gaps, which shrink in the quantum critical region and often vanish at topological phase transitions. This suggests that dissipative stabilization of many-body states, which works directly in the strongly correlated phase with a potentially larger many-body gap, is a promising alternative approach. So far, though, thermalization of synthetic matter into strongly correlated phases has remained largely unexplored.

Recently, photonic systems have emerged as a platform of interest for the exploration of synthetic quantum matter[12–15]. In particular, superconducting circuits have been used to study many-body physics of microwave photons, taking advantage of the individual control of strongly interacting qubits in these circuits. This approach builds on the circuit quantum electrodynamics toolbox developed for quantum computing[16] and has been applied to digital simulation of spin models[17], fermionic dynamics[18] and quantum chemistry[19,20]. Equally of interest are analogue simulation experiments in these circuits, studying low-disorder lattices[21], low-loss synthetic gauge fields[22,23], dissipative lattices[24,25] and many-body localization in disorder potentials[26]. In the circuit platform, the particles that populate the system are microwave photons, which are inevitably subject to intrinsic particle losses. Without an imposed chemical potential, the photonic system eventually decays to the vacuum state, naturally posing the challenge of how to achieve strongly correlated matter in the absence of particle-number conservation. To this end, dissipative preparation and manipulation of quantum states via tailored reservoirs have become an active area of research both theoretically and experimentally, in which dissipative coupling to the environment serves as a resource[27–29]. Such engineered dissipation has been used to stabilize entangled states of ions[30], single-qubit states[31] and entangled two-qubit states[32], and holds promise for autonomous quantum error correction[33–35].

Here, we present a circuit platform for the exploration of quantum matter composed of strongly interacting microwave photons and use it to demonstrate direct dissipative stabilization of a strongly correlated phase of photons. Our scheme[36] builds on and simplifies previous proposals[37–40], and is agnostic to the target phase as long as it is incompressible and exhibits mobile quasi-holes.

To understand the protocol, illustrated in Fig. 1, we consider a target ground state comprising N_0 photons that is spectrally gapped from excited states with the same particle number by the many-body gap Δ_{mb}.

[1]Department of Physics and James Frank Institute, University of Chicago, Chicago, IL, USA. *e-mail: maruichao@gmail.com

Additionally, this state must be incompressible with respect to change in particle number, in the sense that inserting each of the first N_0 particles requires about the same energy, whereas adding the (N_0+1)th particle requires an energy that differs by the compressibility gap Δ_{comp}. Using a combination of coherent drive and engineered dissipation, we irreversibly inject particles into the system near the energy (per particle) of the target state. As long as the target state has good wavefunction overlap with both the initial state (for example, the vacuum $N=0$) and the locally injected particles, the system will be continuously filled until it reaches the target state, at which point further addition of particles is energetically suppressed by Δ_{comp}. Generically, the injected particles will order in the strongly correlated phase under the influence of the underlying coherent interactions, geometries or topological properties of the many-body system. Population of other excited states is highly suppressed by spectral gaps and further made short-lived by engineering an energy-dependent loss that couples only excited manifolds to the environment. The balance of particle injection and loss that is built into the system provides the autonomous feedback that populates the target many-body state, stabilizing it against intrinsic photon loss or accidental excitation.

We realize irreversible particle insertion by coherent injection of pairs of particles into a 'collider', in which they undergo elastic collisions wherein one particle dissipates into an engineered cold reservoir while the other enters the many-body system; loss of the former particle makes this otherwise coherent process irreversible, permanently inserting the latter particle into the system. Previous experiments demonstrating 'optical pumping' into spectrally resolved few-body states[41] relied upon excited-state symmetry to achieve state-dependent dissipation; here we use energy-dependent photon loss to shed entropy—a new approach with broad applicability.

First, we introduce and characterize the photonic Bose–Hubbard circuit; second, we describe and explore an isolated dissipative stabilizer for a single lattice site; and finally we couple the stabilizer to the Bose–Hubbard circuit, realize the stabilization of a Mott insulating phase, and investigate the fate of defects in the stabilized Mott phase.

Building a Bose–Hubbard circuit

Figure 2a shows our circuit, which realizes a one-dimensional Bose–Hubbard lattice for microwave photons, with a Hamiltonian given by:

$$\mathcal{H}_{\mathrm{BH}}/\hbar = -\sum_{\langle ij\rangle} J_{ij} a_i^\dagger a_j + \frac{U}{2}\sum_i n_i(n_i-1) + \sum_i \epsilon_i n_i$$

Here $a_i^\dagger$ is the bosonic creation operator for a photon on site i, J_{ij} is the nearest-neighbour tunnelling rate, U is the on-site interaction, ε_i is the local site energy and $\hbar$ is the reduced Planck constant. Eight transmon qubits[42] constitute the lattice sites of the one-dimensional lattice. Each transmon acts as a nonlinear resonator, where a Josephson junction acts as a nonlinear inductor with Josephson energy E_{J}, in parallel with a cross-shaped metal capacitor with charging energy $E_{\mathrm{c}} = e^2/(2C_\Sigma)$, where e is the electron charge and C_Σ the total capacitance of the transmon. The lattice site has a frequency for the addition of only one photon of $\epsilon = \omega_{01} \approx \sqrt{8E_{\mathrm{J}}E_{\mathrm{c}}}$. The addition of a second photon requires a different amount of energy, with the difference given by the anharmonicity of the transmon, $U = \omega_{12} - \omega_{01} \approx -E_{\mathrm{c}}$. Thus U is the effective two-body on-site interaction for photons on a lattice site. By using tunable transmons where two junctions form a superconducting quantum interference device (SQUID), we control the effective E_{J} and thus the site energy by varying the magnetic flux through the SQUID loop, which is achieved by applying currents to individual galvanically coupled flux-bias lines. Neighbouring lattice sites are capacitively coupled to one another, producing fixed nearest-neighbour tunnelling J.

Each lattice site (transmon) is capacitively coupled to an off-resonant coplanar waveguide readout resonator, enabling site-by-site readout of photon number occupation via the dispersive shift of the resonator. The readout resonators are capacitively coupled to a common transmission line to allow simultaneous readout of multiple lattice sites and thereby

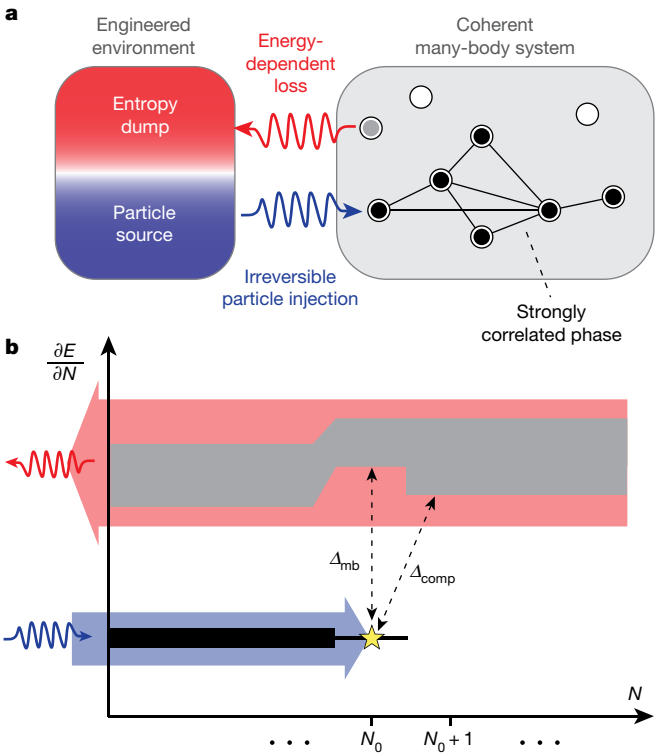

Fig. 1 | Dissipative stabilization of incompressible many-body states. **a**, Entropy and particle flow between the engineered environment and the quantum many-body system. Circles indicate single-particle states of the system; occupied and empty states are shown in black and white, respectively, with grey indicating dissipative depopulation. **b**, Energy required to inject additional photons ($\partial E/\partial N$) as a function of number of photons (N) in the system. Photons are continuously and irreversibly added to the system in a narrow energy-band (blue) that connects the initial vacuum to the desired target state (star) via intermediate states (black region). This process stops when the system is fully filled at photon number N_0 owing to the presence of the compressibility gap Δ_{comp}, thereby preparing and stabilizing the gapped (by energy Δ_{mb}) many-body state in which the photons self-organize into a strongly correlated phase determined by the underlying Hamiltonian. The energy-dependent-loss channels (red) ensure that all excitations into higher-energy states (grey region) are short-lived.

site-resolved microscopy of the lattice. The main contributions to the readout uncertainty are Landau–Zener transfers between neighbouring sites during the ramp to the readout energy and errors from the dispersive readout; see Supplementary Information section E. The readout transmission line also enables charge excitation of all lattice sites.

Site Q_1, at one end of the lattice, is coupled to another resonator that serves as a narrow-band reservoir used for the dissipative stabilization. The reservoir is tunnel-coupled to Q_1 with $J_{\mathrm{R1}} = 2\pi \times 16.3$ MHz and has a linewidth of $\kappa_{\mathrm{R}} = 2\pi \times 9.5$ MHz, obtained by coupling to the 50-Ω environment of the readout transmission line. An additional drive line is capacitively coupled to Q_1 at the end of the lattice to allow direct charge excitation of only Q_1, which is used for dissipative stabilization.

We use transmon qubits with a negative anharmonicity of $U \approx 2\pi \times -255$ MHz, which corresponds to strong attractive interactions, and an on-site frequency tuning range of $\omega_{01} \approx 2\pi \times (3.5–6.0)$ GHz with a tuning bandwidth of 250 MHz. We measure nearly uniform tunnelling rates of about $2\pi \times 6.25$ MHz for J_{23}–J_{78} and $J_{12} = 2\pi \times 12.5$ MHz (J_{12} is designed to optimize the dissipative stabilization). Beyond-nearest-neighbour tunnelling due to residual capacitance between qubits is suppressed by an order of magnitude. The excited-state structure of the transmon gives rise to effective on-site multi-body interaction terms that are irrelevant for the experiments

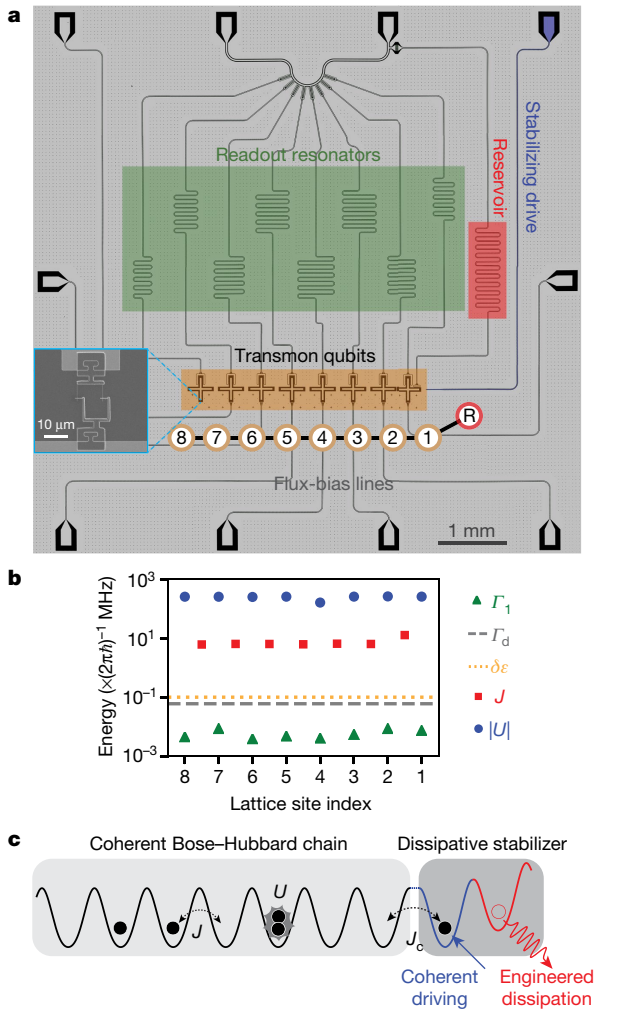

Fig. 2 | Building a Bose–Hubbard lattice in a superconducting circuit. **a**, Optical image of the device. Superconducting transmon qubits (Q_1–Q_8; yellow) constitute lattice sites with energies tunable by individual flux-bias lines. Capacitive coupling between transmons leads to tunnelling J, and transmon anharmonicity gives the on-site interaction U. Readout resonators (green) enable site-resolved occupancy measurement via a common transmission line. A lossy resonator (red) acts as a cold reservoir for the stabilization process. Charge excitation of lattice sites is realized by driving the readout transmission line; a stabilization line (blue) drives only site Q_1. Inset, close-up scanning electron microscope image of the transmon qubit, showing the bottom of the cross-shaped capacitor pad and the SQUID loop. See Supplementary Information for details of the sample parameters and fabrication (section A) and the measurement setup (section B). **b**, Measured on-site interactions U, tunnelling rates J, single-photon losses Γ_1, dephasing rate Γ_d and on-site disorder $\delta\varepsilon$, demonstrating a high-coherence, low-disorder Bose–Hubbard lattice in the strongly interacting regime. Uncertainties in lattice parameters are small compared to site-to-site variations; details in Supplementary Information section F. **c**, The corresponding Bose–Hubbard chain (light grey), coupled at one end to the dissipative stabilizer (dark grey) with coupling J_c. Here we show an implementation of the stabilizer using the reservoir (red) and only one transmon (blue).

presented here, in which the on-site occupancies are predominantly confined to $n = 0, 1, 2$.

We measure single-photon relaxation times of $T_1 \approx 30\ \mu s$ and dephasing times of $T_2^* \approx 3\mu s$ for the lattice sites (see Supplementary Information section F), corresponding to a single-photon loss rate of $\Gamma_1 = 1/T_1 \approx 2\pi \times 5$ kHz and on-site dephasing rate $\Gamma_d = 1/T_2^* \approx 2\pi \times 50$kHz. We have thus realized a highly coherent photonic Bose–Hubbard lattice in the strongly interacting regime $|U| \gg J \gg \Gamma_1, \Gamma_d$, as shown in Fig. 2b. The on-site frequency disorder is another crucial characteristic that should be compared with the other energy scales of the lattice: tunnelling, interaction and, more generally, the many-body gap of the state being studied. We achieve on-site disorder $\delta\varepsilon = \delta\omega_{01} \lesssim 2\pi \times 100$ kHz, well below both J and U, where U is also the approximate excitation gap of the Mott state in the strongly interacting regime[5]. Currently, dephasing Γ_d is limited by electronic noise on the flux bias whereas disorder $\delta\varepsilon$ is limited by precision of the flux-bias calibration (see Supplementary Information section C); neither affects the present experiments.

Dissipative stabilization of a single lattice site

Before examining the more complicated challenge of stabilizing a Bose–Hubbard chain, we consider the following simpler question: how do we stabilize a single lattice site with exactly one photon in the presence of intrinsic single-photon loss? A continuous coherent drive at ω_{01} can at best stabilize the site with an average single-excitation probability of $P_1 = 0.5$ in the steady state, where the $n = 2$ state remains unpopulated because strong interactions make the drive off-resonant for the $1 \rightarrow 2$ transition. To stabilize the site in the $n = 1$ state, one could implement a discrete feedback scheme in which the state of the site is continuously monitored, and whenever the occupation decays from $n = 1$ to $n = 0$, a resonant π pulse injects a single photon into the site. Such active feedback requires constant high-efficiency detection and fast classical control and works only for simple separable states. Here we explore ways to implement such stabilization autonomously by using an engineered reservoir. This autonomous approach has the required feedback built into the driven–dissipative Hamiltonian, enabling the preparation of many-body states with strong and even unknown correlations.

This idea of autonomous stabilization is akin to inverting atoms in laser- or optical-pumping schemes that are prevalent in atomic physics: a coherent optical field continuously drives an atom from the ground state to a short-lived excited state that rapidly decays to a long-lived target state. In the transmon, this means making one photon substantially shorter-lived than the other; to this end, it is helpful to be able to distinguish the two photons, for example, by different spatial wavefunctions or different energies. We take the latter route, harnessing on-site interactions and elastic site-changing collisions to allow the coherent field to add pairs of photons with different energies and the narrow-band reservoir to provide an energy-dependent loss into which the entropy of the lattice site is shed, stabilizing the site into the $n = 1$ state.

We implement two different schemes for stabilizing a single lattice site: the 'one-transmon' and 'two-transmon' schemes. In the one-transmon scheme (Fig. 3a), which is akin to that described in ref. [43], we use the on-site $n = 2$ state and drive a two-photon transition from $n = 0$ to $n = 2$ at frequency $\omega_d = (\omega_{01} + \omega_{12})/2$ and single-photon Rabi rate Ω_d, which is off-resonant with respect to the $n = 1$ state by $U/2$. The $2 \rightarrow 1$ photon loss is realized by coupling the stabilized site to the lossy site (R) at frequency $\omega_R = \omega_{21}$. The optimal stabilization fidelity P_1 (the probability of having on-site photon occupancy $n = 1$) arises from a competition between the coherent pumping rate and various loss processes: at low pumping rates, the photons are not injected fast enough to compete with the one-photon loss Γ_1; at high pumping rates, the lossy site cannot shed the excess photons fast enough and the fidelity is limited by off-resonant coherent admixtures of zero- and two-photon states. The theoretically predicted single-site infidelity $(1 - P_1)$ for optimal lossy channel and driving parameters scales as[36] $(\Gamma_1/|U|)^{1/2}$. The sign of the interaction U does not affect the physics of the experiments described in this paper, because the engineered reservoir is narrow-band and the lattice remains in the strongly interacting regime.

The measured steady-state stabilization fidelity using the one-transmon scheme is shown in Fig. 3b as a function of the driving frequency and strength. Driving the stabilized site resonantly at $\omega_d \approx \omega_{01} = 2\pi \times 4.738$ GHz gives an on-site population that saturates at $P_1 \leq 0.5$, as expected. Near $\omega_d = (\omega_{01} + \omega_{12})/2 = 2\pi \times 4.610$ GHz we observe single-site stabilization and the fidelity increases with driving strength until it reaches an optimal value of $P_1 = 0.81 \pm 0.01$ at $\Omega_d = 2\pi \times 28$ MHz, after which the fidelity drops. Error bars in the

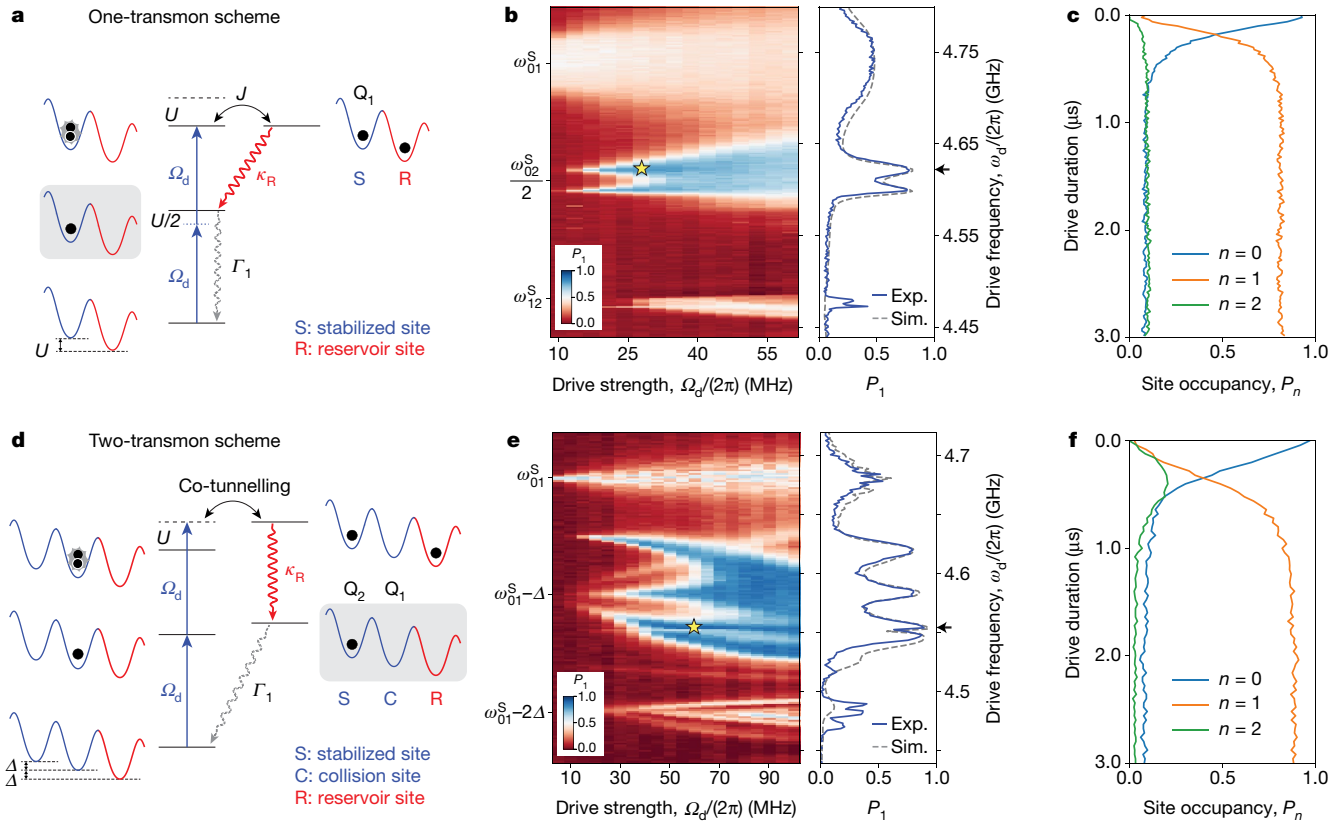

Fig. 3 | Dissipative stabilization of a single lattice site. a, One-transmon scheme. We drive the two-photon transition $0 \rightarrow 2$ at $\omega_d = \omega_{02}/2$, off-resonant with respect to the $n = 1$ state by $U/2$. The $1 \rightarrow 2$ transition is resonant with the reservoir (linewidth κ_R) at $\omega_R = \omega_{21}$ to enhance $\Gamma_{2\rightarrow1}$. This stabilizes the site in the $n = 1$ state (linewidth Γ_1, grey shading). The dashed black line indicates the energy of $n = 2$ without the interaction U. **b**, Measured single-site stabilizer fidelity. Left, stabilizer fidelity, P_1, versus driving frequency, ω_d, and strength, Ω_d, after a drive duration of 3 μs. The optimal observed fidelity is 0.8 ± 0.01 for the one-transmon scheme. Right, measured fidelities ('Exp.') at the optimal Ω_d compared to numerical simulations ('Sim.'), showing quantitative agreement. **c**, Stabilizer filling dynamics. Shown is the occupancy of the stabilized site versus the stabilization time at optimal parameters (star and arrow in **b**). **d**, Two-transmon scheme. Two-transmon sites and the reservoir configured in a ladder (with detuning Δ). Charge-driving at the collision-site frequency injects pairs of photons, which collide elastically and split, with one dissipating in the reservoir and the other being irreversibly injected into the stabilized site. **e**, As in **b**, but for the two-transmon scheme. The optimal observed fidelity for the two-transmon scheme is $P_1 = 0.89^{+0.04}_{-0.01}$. Optimal fidelities in **b** and **e** are both limited predominantly by reservoir thermal population. **f**, As in **c**, but for the two-transmon scheme. The occupancy of the stabilized site is shown versus the stabilization time at optimal parameters (star and arrow in **e**). All data presented in the paper are averages of about 5,000–8,000 independent experimental runs performed at a repetition rate of 4 kHz. For details of the experimental sequence, see Supplementary Information section D. Typical error bars near optimal parameters are $^{+2\%}_{-1\%}$, dominated by readout systematics.

reported fidelities indicate systematic uncertainties at 90% confidence intervals; statistical uncertainties are small, with the standard deviation of the mean being less than 1% (see Supplementary Information section E.3). The split peaks result from resonant coupling between the lossy resonator and the stabilized site, $\omega_R = \omega_{12}$, giving a frequency splitting of $\sqrt{2}J_{R1} \approx 2\pi \times 23$MHz when driving the two-photon transition. The measured data at the optimal Ω_d are plotted in the vertical panel, showing quantitative agreement with a parameter-free numerical model (see Supplementary Information section G). The observed stabilization fidelity is primarily limited by thermal population in the cold reservoir $n_{th}^R = 0.075$, which re-enters the stabilized site (see Supplementary Information section F.4). In Fig. 3c we show the filling dynamics of the stabilization process by plotting the on-site occupancy of the stabilized site versus the duration of the stabilization drive with the optimal driving parameters (star and arrow in Fig. 3b). The single site is filled in about 0.8 μs (with a fitted exponential time constant of 0.19 μs), in agreement with numerical simulations. The finite P_1 at time $t = 0$ arises from the finite qubit temperature in the absence of driving.

In the two-transmon scheme, we use two transmon lattice sites (the 'stabilized site', S and the 'collision site', C) and the lossy resonator (the reservoir, R) in a Wannier–Stark ladder configuration (Fig. 3d). The middle collision site is placed energetically between the stabilized and the reservoir sites, detuned from each by Δ, allowing us to drive the system at the collision site frequency ω_{01}^C and induce elastic collisions that put one photon into the stabilized site and one into the lossy resonator $(2 \times \omega_{01}^C \rightarrow \omega_{01}^S + \omega_R)$. The photon in the reservoir site is quickly lost, leaving the stabilized site in the $n = 1$ state. This scheme resembles evaporative cooling used in ultracold-atom experiments, in which a radiofrequency knife in a magnetic trap provides an energy-dependent loss at the edge of a quantum gas, with elastic collisions causing one particle to gain energy and spill out of the trap while the other particle is cooled[3]. Compared to the one-transmon scheme, the two-transmon scheme provides an additional degree of freedom, making it possible to separate the effective pumping rate from the detuning, thus enabling better stabilization performance where the optimal infidelity scales as[36] $(\Gamma_1/|U|)^{2/3}$. In addition, the stabilized site is not driven directly in the two-transmon scheme, thus avoiding infidelities from off-resonant population of higher transmon levels.

The measured steady-state fidelity of the stabilized site in the two-transmon scheme is shown in Fig. 3e with $\Delta = 2\pi \times 100$ MHz, chosen for optimal fidelity. The expected stabilization peak at the collision-site frequency $\omega_d = \omega_{01}^C = \omega_{01}^S - \Delta$ is observed, accompanied by other features with high P_1 from higher-order collision processes[44] (see Supplementary Information section G.1). The measured optimal single-site stabilizer fidelity is $P_1 = 0.89^{+0.04}_{-0.01}$ at $\Omega_d = 2\pi \times 60$ MHz and

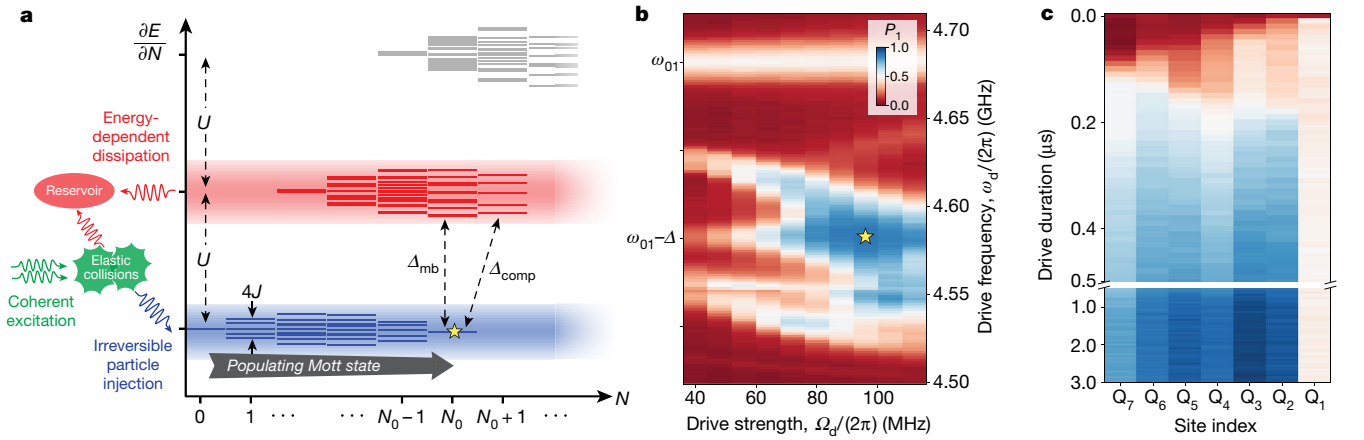

Fig. 4 | Dissipative stabilization of a Mott insulator. a, Many-body spectrum of a strongly interacting Bose–Hubbard chain, showing bands separated by the interaction U. Particles are injected into the system's hole band (blue shading) via a two-photon collision that irreversibly sends one photon into the reservoir and the other into the system. The lattice is filled up to and stabilized in the $n = 1$ Mott state (grey arrow), which is both gapped (Δ_{mb}) and incompressible (Δ_{comp}). The reservoir also absorbs excitations to higher-energy states (red shading). For $|U| \gg J$, this approach also applies for $U < 0$. **b**, Mott fidelity. The stabilizer in the two-transmon scheme is coupled to the end of a five-site Bose–Hubbard chain. The measured steady-state P_1, averaged over sites $Q_2 - Q_7$, is shown versus the stabilization-drive frequency and strength, exhibiting the same qualitative features as in Fig. 3e. We achieve an optimal Mott fidelity of $0.88^{+0.03}_{-0.01}$ for resonant driving of the collision site with $\Omega_d = 2\pi \times 95$ MHz (indicated by the star). **c**, Mott filling dynamics. Starting with an empty lattice, we plot P_1 on each site versus the duration of the stabilization drive at optimal driving parameters. Panels **b** and **c** share the same colour scale. Injected particles exhibit light-cone-like ballistic transport across the lattice and subsequent reflection off of the far end of the lattice. Steady-state Mott filling is reached in about 0.8 μs.

$\omega_d = 2\pi \times 4.555$ GHz. Both the measured steady-state fidelity and the stabilizer dynamics (Fig. 3f) are in quantitative agreement with numerical simulation, with the highest observed fidelity primarily limited by reservoir thermal population. We note that compared to the one-transmon scheme, the two-transmon scheme yields higher fidelities and does so over a broader parameter range (for example, the $\omega_d \approx \omega_{01}^S - \Delta$ peak at higher Ω_d); it is thus better suited to stabilize many-body states, in which rapid refilling over a finite density of states is required, as described in the next section.

Stabilization of a Mott insulator

Having demonstrated our ability to stabilize a lattice site with a single photon, we now use it to stabilize many-body states in the Bose–Hubbard chain. The single stabilized site acts as a spectrally narrow-band photon source that is continuously replenished. Photons from this site sequentially tunnel into, and gradually fill, the many-body system, until the addition of further photons requires an energy different from that of the source, resulting in ordering of the photons by their strong coherent interaction into a Mott insulator with near-perfect site-to-site particle-number correlation in the Hubbard chain[5].

For this stabilization method to work, the target phase must satisfy certain conditions, illustrated for the current system in Fig. 4a. The phase should be incompressible with respect to particle addition[36]: Once the target state is reached, the stabilizer should be unable to inject additional photons into the system; at the same time, when a photon is lost from the target state (owing to decay into the environment), the stabilizer must refill the hole defect efficiently. This requires the hole- and particle-excitation spectra of the target state to be spectrally separated (with a gap of about Δ_{comp}). In addition, when refilling a hole, we must avoid driving the system into excited states with the same number of photons as the target state—this requires the target phase to exhibit a many-body gap Δ_{mb}. The stabilizer, as a continuous photon source, thus needs to be narrow-band compared to both the many-body gap and the gap between the hole states and the particle states, but sufficiently broad-band to address all of the hole states spectroscopically. The performance of the many-body stabilizer is then determined by how efficiently the hole defects in the many-body state can be refilled—a combined effect of the repumping rate of the single-site stabilizer at energy ε_k (where k is the quasi-momentum of the hole) and the wavefunction overlap between the defect state and the stabilizer site.

We tunnel-couple the demonstrated single-site stabilizer to one end of the Bose–Hubbard chain and attempt to stabilize the $n = 1$ Mott insulator of photons. The Mott state is a gapped ground state[5] that satisfies the incompressibility requirements[45]. The many-body gap is set by the cost of creating doublon–hole excitations on top of the Mott state, about U. Particle-like excitations are gapped by the strong interaction (about U for the $n = 1$ Mott state), whereas hole excitations follow the single-particle dispersion, with energies lying in a band of $|\epsilon_k| \leq 2J$ in the one-dimensional lattice, providing clear spectral separation in the Mott limit ($|U| \gg J$). For a homogeneous lattice, all hole eigenstates are delocalized across the lattice, making it possible to use a single stabilizer at one end of the chain. The amplitude of the defect-state wavefunctions at the stabilizer can be adjusted via the coupling between the chain and the stabilizer, J_c. Here we attach an additional five-site chain ($Q_3 - Q_7$) to a two-transmon stabilizer that stabilizes Q_2. All lattice sites are tuned to the same energy as Q_2. The coupling between the stabilizer and the rest of the chain is $J_c \approx J_{chain} \approx 2\pi \times 6.25$ MHz.

In Fig. 4b, we plot the measured steady-state Mott fidelity ($\langle P_1 \rangle$, chain-averaged over sites $Q_2 - Q_7$) as a function of the stabilization-drive frequency and strength, after a driving duration of 5 μs. The optimal Mott fidelity of $0.88^{+0.03}_{-0.01}$ is achieved by driving at $\omega_d = \omega_{01} - \Delta$ with $\Omega_d = 2\pi \times 96$ MHz, demonstrating a dissipatively stabilized photonic Mott insulator in which the on-site number fluctuations are strongly suppressed. The observed defects within the chain are predominantly holes ($P_0 \approx 0.10$) with very low doublon probabilities ($P_2 \approx 0.02$; see Supplementary Information section E.3). Ignoring small site-to-site variations in the Mott fidelity, we obtain the on-site number fluctuation of the Mott state $\delta n \equiv \sqrt{\langle n^2 \rangle - \langle n \rangle^2} = 0.34^{+0.01}_{-0.05}$, or a configuration entropy of $s \equiv -k_B \sum_n P_n \ln(P_n) = 0.42^{+0.04}_{-0.12} k_B$ per site, where k_B is the Boltzmann constant. Figure 4b shows qualitatively the same features as the single-site stabilization in Fig. 3d. Near $\omega_d \approx \omega_{01}^C$, the performance of the single-particle stabilizer is robust over variations in both drive detuning, which gives good energetic overlap with the hole-defect states of the Mott phase that span a frequency range of $4J \approx 2\pi \times 25$ MHz, and drive strength, which provides the high repumping rates necessary to fill the whole lattice without sacrificing stabilizer fidelity. For larger lattices with a single stabilizer site, the stabilization performance will eventually be limited by the reduced

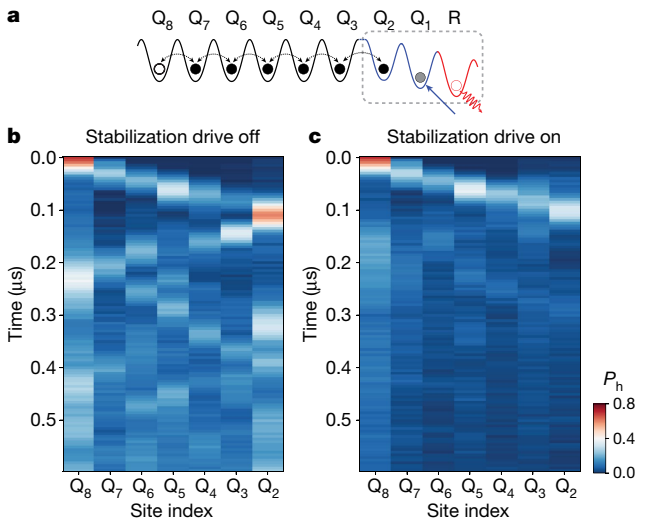

Fig. 5 | Dynamics of a hole defect in the Mott insulator. a, To explore thermalization dynamics near the steady state, we prepare a Mott insulator using the two-transmon stabilizer (grey box) while site Q_8 is energetically detuned to create a localized hole defect at the end of the lattice opposite the stabilizer. Q_8 is then brought into resonance with the rest of the lattice, and we observe how the defect propagates and the chain refills. Depicted is the state at the beginning of this process, with occupied (empty) sites shown in black (white). **b**, Excess-hole density, P_h, versus evolution time in the absence of the stabilization drive. The hole propagates through the otherwise filled Mott insulator, exhibiting a coherent quantum walk. **c**, With the stabilization drive on during the evolution, the hole shows the same ballistic propagation until it reaches the stabilizer, where it is efficiently refilled.

refilling rate for the increasing number of sites or modes and by disorder-induced localization that inhibits the effective refilling of defects away from the stabilizer site. Multiple stabilizers may be used to circumvent such limitations, as suggested in previous studies[37,46] that proposed each lattice site to be coupled to a driven–dissipative bath.

In Fig. 4c we plot the time dynamics of all lattice sites in the Hubbard chain as the Mott state is filled from vacuum, at the optimal driving parameter (indicated with the yellow star in Fig. 4b). The initial filling dynamics reveal near-ballistic propagation of injected photons after they enter the lattice from the stabilizer, consistent with the dispersion of a localized wavepacket continuously injected at the stabilized site that undergoes quantum tunnelling in the lattice. We observe light-cone-like transport[47] at a speed of approximately $2J \approx 78$ sites per microsecond (13 ns per site). In comparison, the single-site refilling time at these Mott driving parameters (Fig. 3e) is about 45 ns and remains relatively uniform over the lattice bandwidth of $4J$. It is natural to ask how our dissipatively prepared Mott state relates to the corresponding Mott state in an isolated system at equilibrium. Fundamentally, this is a question of the timescales between thermalization within the system and interaction with the reservoir. In future work, we can measure density–density correlations or entanglement[48] to compare the dissipatively prepared Mott insulator to an equilibrium Mott insulator at finite temperature and investigate how the stabilized wavefunctions vary with distance from the stabilizer.

Finally, we examine the near-steady-state dynamics of the stabilized chain by preparing a single defect and watching it refill (Fig. 5). We begin by preparing the dissipatively stabilized Mott insulator in Q_2–Q_7 with Q_8 sufficiently energetically detuned so that it remains empty. Q_8 is then rapidly tuned to resonance with the rest of the lattice, and the population of holes (excess $n = 0$ population, compared to the steady-state Mott population, $P_h = P_0 - P_0^{Mott}$) is measured across the chain after a variable evolution time. In the absence of a stabilization drive during the evolution of the hole (Fig. 5b), we observe the coherent propagation of the hole defect (consistent with theory; see Supplementary Information section G.3). The wavefront traverses the lattice at a speed of $2J$ at short times, whereas at longer times we observe complex structures emerge owing to coherent interference of multiple reflections off the edges of the lattice. On the other hand, when the stabilization drive remains on during the evolution of the hole defect (Fig. 5c), we observe similar initial ballistic propagation until the defect reaches the stabilizer, where the hole defect is immediately filled. We note that the many-body filling front in Fig. 4c is essentially as fast as the single-hole propagation shown in Fig. 5c.

Conclusions

We have constructed a Bose–Hubbard lattice for microwave photons in superconducting circuits. Transmon qubits serve as individual lattice sites where the anharmonicity of the qubits provides strong on-site interaction, and capacitive coupling between qubits leads to fixed nearest-neighbour tunnelling. The long coherence times of the qubits, together with the precise dynamical control of their transition frequencies, make this device an ideal platform for exploring quantum materials. Using readout resonators dispersively coupled to each lattice site, we achieve time- and site-resolved detection of the lattice occupancy. Frequency-multiplexed, simultaneous readout of multiple lattice sites[49] could be implemented in future experiments to enable direct measurement of entanglement and emergence of many-body correlations.

We further demonstrate a dissipative scheme to populate and stabilize gapped, incompressible phases of strongly interacting photons—used here to realize the first Mott insulator of photons. The combination of coherent driving and engineered dissipation creates a tailored reservoir that continuously replenishes the many-body system with low-entropy photons, which then self-organize into a strongly correlated phase. Furthermore, the reservoir acts as an entropy dump for any excitation on top of the target phase. The dissipatively prepared incompressible phases can serve as a starting point for exploring other strongly correlated phases via coherent adiabatic passages, including compressible ones. The latter have also been proposed to be accessible directly with dissipative preparation[38,40].

This platform opens up numerous avenues for future exploration; for example regarding the optimal spectral or spatial distribution of engineered reservoirs; how this depends on the excitation spectrum of the isolated model under consideration; how the equilibrium properties of the dissipatively stabilized system relate to those of the isolated system; how higher-order correlations emerge and thermalize; and what thermodynamic figures of merit can be achieved for the reservoir and its coupling to the system.

Finally, our results provide a path towards topologically ordered matter using related tools, for example, the creation of fractional quantum Hall states of photons[50,51] in recently realized low-loss microwave Chern insulator lattices[23]. The unique ability of circuit models to realize exotic real-space connectivity[52] further suggests the possibility of exploring topological fluids on reconfigurable higher-genus surfaces—a direct route to anyonic braiding[53].

Data availability

The experimental data and numerical simulations presented in this manuscript are available from the corresponding author upon request.

Online content

Any methods, additional references, Nature Research reporting summaries, source data, statements of data availability and associated accession codes are available at https://doi.org/10.1038/s41586-019-0897-9.

Received: 30 July 2018; Accepted: 7 December 2018;
Published online 6 February 2019.

1. Bakr, W. S., Gillen, J. I., Peng, A., Folling, S. & Greiner, M. A quantum gas microscope for detecting single atoms in a Hubbard-regime optical lattice. *Nature* **462**, 74–77 (2009).
2. Sherson, J. F. et al. Single-atom-resolved fluorescence imaging of an atomic Mott insulator. *Nature* **467**, 68–72 (2010).
3. Anderson, M. H. et al. Observation of Bose–Einstein condensation in a dilute atomic vapor. *Science* **269**, 198–201 (1995).

4. Davis, K. B. et al. Bose–Einstein condensation in a gas of sodium atoms. *Phys. Rev. Lett.* **75**, 3969–3973 (1995).
5. Greiner, M., Mandel, O., Esslinger, T., Hänsch, T. W. & Bloch, I. Quantum phase transition from a superfluid to a Mott insulator in a gas of ultracold atoms. *Nature* **415**, 39–44 (2002).
6. Simon, J. et al. Quantum simulation of antiferromagnetic spin chains in an optical lattice. *Nature* **472**, 307–312 (2011).
7. Mazurenko, A. et al. A cold-atom Fermi–Hubbard antiferromagnet. *Nature* **545**, 462–466 (2017).
8. He, Y.-C., Grusdt, F., Kaufman, A., Greiner, M. & Vishwanath, A. Realizing and adiabatically preparing bosonic integer and fractional quantum Hall states in optical lattices. *Phys. Rev. B* **96**, 201103 (2017).
9. Gring, M. et al. Relaxation and prethermalization in an isolated quantum system. *Science* **337**, 1318–1322 (2012).
10. Schreiber, M. et al. Observation of many-body localization of interacting fermions in a quasirandom optical lattice. *Science* **349**, 842–845 (2015).
11. Kaufman, A. M. et al. Quantum thermalization through entanglement in an isolated many-body system. *Science* **353**, 794–800 (2016).
12. Greentree, A. D., Tahan, C., Cole, J. H. & Hollenberg, L. C. L. Quantum phase transitions of light. *Nat. Phys.* **2**, 856–861 (2006).
13. Noh, C. & Angelakis, D. G. Quantum simulations and many-body physics with light. *Rep. Prog. Phys.* **80**, 016401 (2016).
14. Hartmann, M. J. Quantum simulation with interacting photons. *J. Opt.* **18**, 104005 (2016).
15. Gu, X., Kockum, A. F. & Miranowicz, A., Liu, Y. & Nori, F. Microwave photonics with superconducting quantum circuits. *Phys. Rep.* **718–719**, 1–102 (2017).
16. Wallraff, A. et al. Strong coupling of a single photon to a superconducting qubit using circuit quantum electrodynamics. *Nature* **431**, 162–167 (2004).
17. Salathé, Y. et al. Digital quantum simulation of spin models with circuit quantum electrodynamics. *Phys. Rev. X* **5**, 021027 (2015).
18. Barends, R. et al. Digital quantum simulation of fermionic models with a superconducting circuit. *Nat. Commun.* **6**, 7654 (2015).
19. O'Malley, P. et al. Scalable quantum simulation of molecular energies. *Phys. Rev. X* **6**, 031007 (2016).
20. Kandala, A. et al. Hardware-efficient variational quantum eigensolver for small molecules and quantum magnets. *Nature* **549**, 242–246 (2017).
21. Underwood, D. L., Shanks, W. E., Koch, J. & Houck, A. A. Low-disorder microwave cavity lattices for quantum simulation with photons. *Phys. Rev. A* **86**, 023837 (2012).
22. Roushan, P. et al. Chiral ground-state currents of interacting photons in a synthetic magnetic field. *Nat. Phys.* **13**, 146–151 (2017).
23. Owens, C. et al. Quarter-flux Hofstadter lattice in a qubit-compatible microwave cavity array. *Phys. Rev. A* **97**, 013818 (2018).
24. Raftery, J., Sadri, D., Schmidt, S., Türeci, H. E. & Houck, A. A. Observation of a dissipation-induced classical to quantum transition. *Phys. Rev. X* **4**, 031043 (2014).
25. Fitzpatrick, M., Sundaresan, N. M., Li, A. C., Koch, J. & Houck, A. A. Observation of a dissipative phase transition in a one-dimensional circuit QED lattice. *Phys. Rev. X* **7**, 011016 (2017).
26. Roushan, P. et al. Spectroscopic signatures of localization with interacting photons in superconducting qubits. *Science* **358**, 1175–1179 (2017).
27. Poyatos, J., Cirac, J. & Zoller, P. Quantum reservoir engineering with laser cooled trapped ions. *Phys. Rev. Lett.* **77**, 4728–4731 (1996).
28. Plenio, M. B., Huelga, S. F., Beige, A. & Knight, P. L. Cavity-loss-induced generation of entangled atoms. *Phys. Rev. A* **59**, 2468–2475 (1999).
29. Biella, A. et al. Phase diagram of incoherently driven strongly correlated photonic lattices. *Phys. Rev. A* **96**, 023839 (2017).
30. Barreiro, J. T. et al. An open-system quantum simulator with trapped ions. *Nature* **470**, 486–491 (2011).
31. Lu, Y. et al. Universal stabilization of a parametrically coupled qubit. *Phys. Rev. Lett.* **119**, 150502 (2017).
32. Shankar, S. et al. Autonomously stabilized entanglement between two superconducting quantum bits. *Nature* **504**, 419–422 (2013).
33. Kapit, E., Chalker, J. T. & Simon, S. H. Passive correction of quantum logical errors in a driven, dissipative system: a blueprint for an analog quantum code fabric. *Phys. Rev. A* **91**, 062324 (2015).
34. Kapit, E. Hardware-efficient and fully autonomous quantum error correction in superconducting circuits. *Phys. Rev. Lett.* **116**, 150501 (2016).
35. Albert, V. V. et al. Pair-cat codes: autonomous error-correction with low-order nonlinearity. Preprint at https://arxiv.org/abs/1801.05897 (2018).
36. Ma, R., Owens, C., Houck, A., Schuster, D. I. & Simon, J. Autonomous stabilizer for incompressible photon fluids and solids. *Phys. Rev. A* **95**, 043811 (2017).
37. Kapit, E., Hafezi, M. & Simon, S. H. Induced self-stabilization in fractional quantum Hall states of light. *Phys. Rev. X* **4**, 031039 (2014).
38. Hafezi, M., Adhikari, P. & Taylor, J. Chemical potential for light by parametric coupling. *Phys. Rev. B* **92**, 174305 (2015).
39. Lebreuilly, J., Wouters, M. & Carusotto, I. Towards strongly correlated photons in arrays of dissipative nonlinear cavities under a frequency-dependent incoherent pumping. *C. R. Phys.* **17**, 836–860 (2016).
40. Lebreuilly, J. et al. Stabilizing strongly correlated photon fluids with non-Markovian reservoirs. *Phys. Rev. A* **96**, 033828 (2017).
41. Hacohen-Gourgy, S., Ramasesh, V. V., De Grandi, C., Siddiqi, I. & Girvin, S. M. Cooling and autonomous feedback in a Bose–Hubbard chain with attractive interactions. *Phys. Rev. Lett.* **115**, 240501 (2015).
42. Koch, J. et al. Charge-insensitive qubit design derived from the Cooper pair box. *Phys. Rev. A* **76**, 042319 (2007).
43. Leek, P. et al. Using sideband transitions for two-qubit operations in superconducting circuits. *Phys. Rev. B* **79**, 180511 (2009).
44. Ma, R. et al. Photon-assisted tunneling in a biased strongly correlated Bose gas. *Phys. Rev. Lett.* **107**, 095301 (2011).
45. Gemelke, N., Zhang, X., Hung, C.-L. & Chin, C. In situ observation of incompressible Mott-insulating domains in ultracold atomic gases. *Nature* **460**, 995 (2009).
46. Verstraete, F., Wolf, M. M. & Cirac, J. I. Quantum computation and quantum-state engineering driven by dissipation. *Nat. Phys.* **5**, 633–636 (2009).
47. Cheneau, M. et al. Light-cone-like spreading of correlations in a quantum many-body system. *Nature* **481**, 484–487 (2012).
48. Islam, R. et al. Measuring entanglement entropy in a quantum many-body system. *Nature* **528**, 77–83 (2015).
49. Jeffrey, E. et al. Fast accurate state measurement with superconducting qubits. *Phys. Rev. Lett.* **112**, 190504 (2014).
50. Umucalilar, R. & Carusotto, I. Fractional quantum Hall states of photons in an array of dissipative coupled cavities. *Phys. Rev. Lett.* **108**, 206809 (2012).
51. Anderson, B. M., Ma, R., Owens, C., Schuster, D. I. & Simon, J. Engineering topological many-body materials in microwave cavity arrays. *Phys. Rev. X* **6**, 041043 (2016).
52. Ningyuan, J., Owens, C., Sommer, A., Schuster, D. & Simon, J. Time- and site-resolved dynamics in a topological circuit. *Phys. Rev. X* **5**, 021031 (2015).
53. Barkeshli, M. & Qi, X.-L. Topological nematic states and non-Abelian lattice dislocations. *Phys. Rev. X* **2**, 031013 (2012).

Acknowledgements We thank M. Hafezi and A. Houck for discussions. This work was supported by Army Research Office grant W911NF-15-1-0397 and by the University of Chicago Materials Research Science and Engineering Center (MRSEC), which is funded by the National Science Foundation (NSF) under award number DMR-1420709. D.I.S. acknowledges support from the David and Lucile Packard Foundation; R.M. acknowledges support from the MRSEC-funded Kadanoff-Rice Postdoctoral Research Fellowship; C.O. is supported by the NSF Graduate Research Fellowships Program. This work made use the Pritzker Nanofabrication Facility at the University of Chicago, which receives support from NSF ECCS-1542205.

Reviewer information *Nature* thanks A. Daley, K. Hazzard and the other anonymous reviewer(s) for their contribution to the peer review of this work.

Author contributions R.M., B.S., C.O., J.S. and D.I.S. designed and developed the experiments. R.M. and B.S. performed the device fabrication, measurements and analysis, with assistance from N.L. and Y.L. All authors contributed to the preparation of the manuscript.

Competing interests The authors declare no competing interests.

Additional information
Supplementary information is available for this paper at https://doi.org/10.1038/s41586-019-0897-9.
Reprints and permissions information is available at http://www.nature.com/reprints.
Correspondence and requests for materials should be addressed to R.M.
Publisher's note: Springer Nature remains neutral with regard to jurisdictional claims in published maps and institutional affiliations.